Supplementary Data

Materials and Methods

Chromitite samples from the Black Thor chromite deposit, Ontario, Canada were obtained from Ontario Geological Survey. The Black Thor chromite deposit is a sill like intrusion found within the "Ring of Fire" intrusive suite, located in the Neoarchean Mcfaulds lake greenstone belt (Laarman, 2013). The intrusion hosting the Black Thor deposit consists of cyclically layered ultramafic rocks, beginning with olivine rich lithologies (dunite to peridotite) and progressing upward to more pyroxene rich lithologies (olivine pyroxenite, feldspathic pyroxenite and gabbro). The Black Thor deposit is the most extensive chromite zone in the intrusion and occurs as large thickly bedded chromittite layers at the transition from olivine rich to pyroxene rich lithologies (Weston and Shinkle, 2013; Laarman, 2013)

Reagents for the long-term batch experiments

The interaction of chromite nanoparticles with hausmannite nanoparticles was studied in the absence and presence of chamosite and organic rich soil (Table 2). Chamosite samples from the Michigamme mine, Michigan, USA were purchased from "Rogers Minerals" and crushed in a ring mill to a powder containing predominantly silt sized grains. Chamosite [$(Fe_{3.9}Mg_{0.62}Al_{0.48})Al(Si_3Al)O_{10}(OH)_8$] is a Fe-rich endmember of the clinochlore-chamosite solid solution and a common mineral in serpentinites and ultramafic rocks (Siebecker et al., 2018). Organic rich podzolic soil (contact pH = 5.5) was sampled in a wooded area close to the township of Massey, Ontario (49°19'58.36"N, -82°02'57.24"W). After removal of the larger debris (leaves, sticks) the soil was crushed with a mortar and pestle to a silt-size powder. Hausmannite (Mn_3O_4) nanoparticles were purchased from the company "US Research Nanomaterials, Inc". Their pre-

characterization with TEM indicated an average particle size with diameters of 50 ± 5nm. Table S1 and Figures S1-S3 list the chemical compositions and powder diffraction pattern of the chamosite powder, organic-rich soil and hausmannite nanoparticles.

Table S1: XRF analysis of the organic rich soil and chamosite powder used in the long-term batch experiments.

Oxide	Chamosite powder (wt%)	Organic rich soil (wt%)
Al2O3	18.28	10.3
BaO	<0.004	0.049
CaO	0.536	1.33
Cr2O3	0.023	0.006
Fe2O3	44.95	3.12
K2O	0.56	1.91
MgO	3.63	0.8
MnO	0.918	0.032
Na2O	0.02	2.36
Nitrogen 105	0.07	1.9
P2O5	0.011	0.108
SiO2	24.96	60.18
TiO2	1.91	0.43
Total	99.45	99.22
Total LOI	3.65	18.6

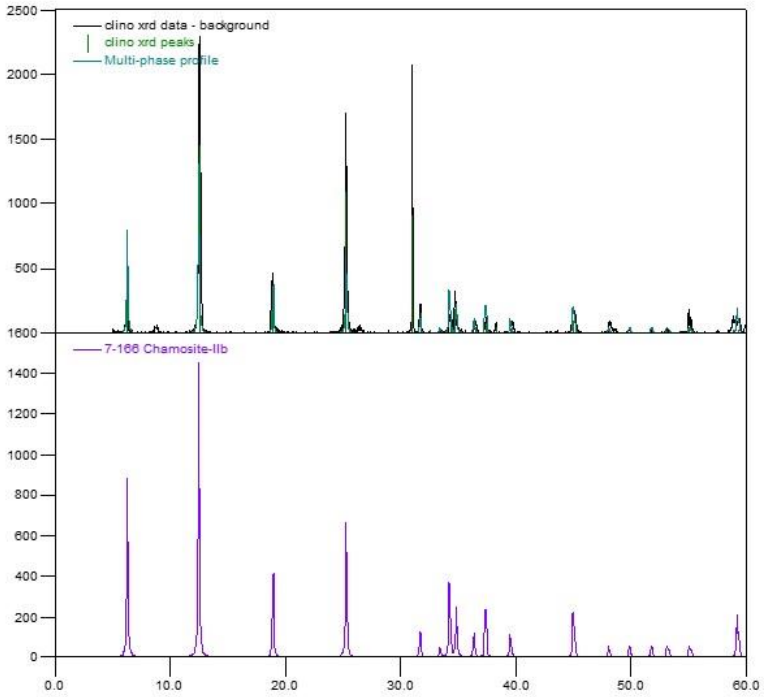

Fig. S1. X-ray diffraction pattern of the chamosite powder used in the long term batch experiments. The top pattern shows the observed diffraction pattern (black) and the pattern for chamosite (green) which is also shown on the bottom (violet).

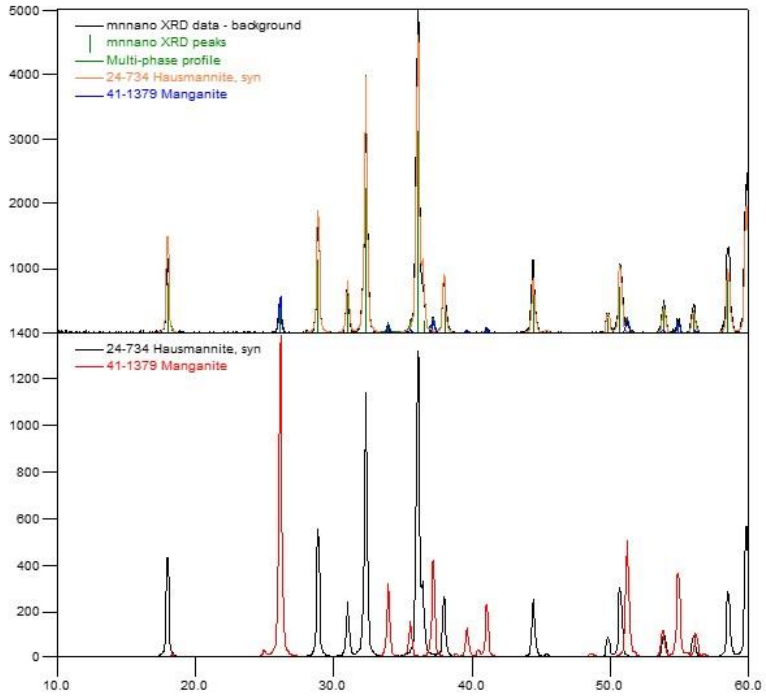

Fig. S2. X-ray diffraction pattern of the hausmannite and manganite nanoparticle powder used in the long term batch experiments. The top pattern shows the observed diffraction peaks (black), the diffraction pattern for hausmannite and manganite and their sum (green). The individual pattern for hausmannite and magnaite are shown at the bottom.

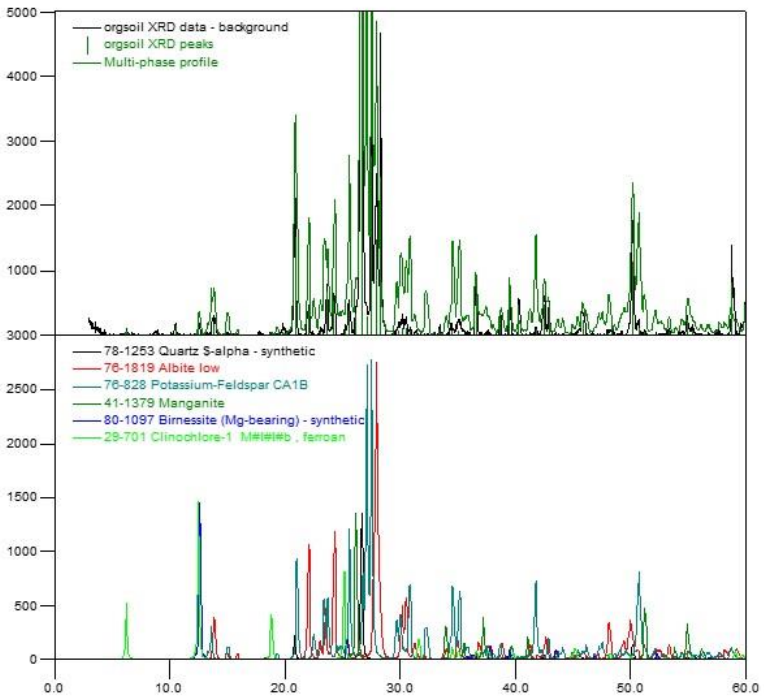

Fig. S3. X-ray diffraction pattern of the organic rich soils used in the long term batch experiments (black) and the sum of pattern of all identified phases (green). The individual pattern of all identified phases are shown at the bottom

Synthesis of the chromite nanoparticles

The chromite nanoparticles for these experiments were synthesised with sizes similar to those observed in the Cr-rich silicates. The synthesis followed a modified variation of the coprecipitation method used by Matulkova et al. (2015) and Edrissi et al (2011). Stoichiometric amounts of $Cr(NO_3) \bullet 9H_2O$ and $FeCl_2$ (Cr : Fe = 2:1) were dissolved into 50ml of distilled water. This solution was then mixed with 100ml of distilled water containing glycerol as a capping agent (5% in distilled water) under constant stirring. Ammonium hydroxide precipitating agent was added dropwise until the pH was adjusted to pH = 11-12. The precipitates were then centrifuged and washed with distilled water several times and then dried at around 40^{o}C. Lastly, the precipitates were calcinated in a vacuum sealed glass tube (< 100 mTorr) at 600^{o}C for 2 hours.

Coprecipitation [1] and calcination [2] reaction can be formulated as follows:

$$2Cr(NO_3)_3 + FeCl_2 + 8NH_4OH \rightarrow 2Cr(OH)_3 + Fe(OH)_2 + 6NH_4NO_3 + 2NH_4Cl \quad [1]$$

$$2Cr(OH)_3 + Fe(OH)_2 \rightarrow FeCr_2O_4 \quad [2]$$

Powders of chromite nanoparticles from two syntheses were mixed and treated in an ethanol-based ultra-sonic bath for 2 hours in order to reduce the size of the nanoparticle aggregates.

TEM images of the synthesized chromite nanoparticles show the occurrence of individual nanoparticles and aggregates of nanoparticles with Fe and Cr homogeneously distributed with the chromte nanoparticles (average Cr : Fe atomic ratio: 1.8 : 1). (Fig. S4). The chromite nanoparticles have diameters between 5 and 15 nm (Fig S1a-e) and are thus similar in size as the chromite nanoparticles in the Cr-rich silicates of the chromitites (Schindler et al. 2017

Analysis of Cr in the solute and colloidal fractions after the leaching and batch experiments

The elemental concentrations of Mg, Al, Si, Cr, and Fe in the solutions after the leaching experiments with the silicate-enriched chromitite powders were determined with solution-mode inductively coupled plasma mass emission spectrometry (ICP-MS) at Geolabs, Sudbury, Ontario, Canada. The leachates were filtered with a 450 nm filter and acidified with HNO_3. Blanks, sample replicates, duplicates and internal reference materials, both aqueous and geochemical standards are routinely used in the laboratory as part of the quality assurance.

The long-term batch experiments were conducted in collaboration with the Ministry of the Environment, Conservation and Parks laboratory services branch (MECP). Due to analytical problems in the MECP lab, all chemical analyses were conducted three months after the TEM studies (i.e. after nine months). Ten millilitres from each batch experiment were filtered with a 0.45 µm Whatman filter cartridge using a 10 mL Luer Lock Syringe. The solutions were treated with an *aqua regia* digest (following method E3470 of the MECP) and analysed for major and trace elements with a Perkin Elmer Optima 4300 DV ICP-OES.

The concentrations of Cr^{3+} and Cr^{6+} in the leachate without (the majority of) nanoparticles were determined using a modified version of the method 6800 of the MECP laboratory services branch:

1. After filtering, 50 mL of each sample were mixed with 0.29 gr NaCl (0.1 $molL^{-1}$ NaCl solution) in order to promote the aggregation of the remaining chromite- and hausmannite nanoparticles and to desorb any adsorbed Cr^{3+} and Cr^{6+} aqueous species from the surfaces of the solid material.
2. The solutions were subsequently centrifuged at 5000 rpm for 4 hours, which should have deposited particles or aggregates of nanoparticles with diameters larger than 35 nm;

3. The solutions were then diluted by a factor ten and 100 µL of each solution was added to 9.9 mL of a 2 mmolL^{-1} EDTA solution of pH 5 (in order to complex Cr^{3+} and thus preventing its oxidation);
4. These solutions were spiked with a Cr-50 enriched Cr^{3+}-solution containing 100 µL^{-1} Cr and a Cr-53-enriched Cr^{6+}-solution containing 100 µL^{-1} Cr; an analytical step that allows to monitor any potential changes in the Cr^{3+} and Cr^{6+} concentrations over time;
5. The spiked solutions were heated at 70°C for 40 min and then transferred to a chromatography vial for analysis with an Analytik Jena 820MS ICP-MS with a CRI skimmer cone and a standard sampler cone.

Additionally, 50 ml from each batch experiment were analysed (without the addition of NaCl) at the ALS environmental laboratories. The solutions were treated and preserved with NaOH and an ammonium sulfate/ammonium hydroxide buffer. Subsequent chromatography using a Thermo Scientific Dionex Aquion IC resulted in the separation of CrO_4^{2-} anions from other Cr-bearing species and chromite nanoparticles. The CrO_4^{2-} -bearing solution was treated with diphenylcarbazide (DPC), a colour reagent, which resulted in the simultaneous oxidation of diphenylcarbazide to diphenylcarbazone, the reduction of Cr^{6+} to Cr^{3+} and the chelation of Cr^{3+} by diphenylcarbazone. The concentrations of the latter chelate was determined with UV-VIS spectroscopy at 530 nm.

Powder X-ray powder diffraction, X-ray Fluorescence Spectroscopy and Loss of Ignition

Powder X-ray powder diffraction pattern of chromitite samples and reagents used in the experiments listed above were recorded with an automated Philips PW 1729 X-ray diffractometer and a Bruker D 5000 system using Co Kα (1.79 Å) and Cu radiation (1.54 Å),

respectively. X-ray diffraction patterns from powdered samples were collected at a voltage of 40 kV and current of 30 mA over a scan range of 5-65° 2θ and with a step size of 0.02° 2θ and a dwell time of 2 s per step.

Samples of chamosite, chromitite and silicate-enriched fraction were fused with a borate flux to produce glass beads for characterization by X-ray Fluorescence Spectroscopy (XRF). The glass beads were subsequently analyzed with a Panalytical Axios Advanced XRF spectrometer.

References

Edrissi, M., Hosseini, S. A., and Soleymani, M. (2011) Synthesis and characterisation of copper chromite nanoparticles using coprecipitation method. Micro & Nano Letters, 6, 836-839.

Laarman, J. E. (2013) A detailed metallogenic study of the McFaulds Lake chromite deposits, northern Ontario. Ph.D. thesis, The University of Western Ontario, pp 494.

Matulkova, I., Holec, P., Pacakova, B., Kubickova, S., Mantlikova, A., Plocek, J., Nemec, I., Niznansky, D., and Vejpravova, J. (2015). On preparation of nanocrystalline chromites by co-precipitation and autocombustion methods. Materials Science and Engineering: B, 195, 66-73.

Schindler, M., Berti, D., and Hochella, M. F. (2017). Previously unknown mineral-nanomineral relationships with important environmental consequences: The case of chromium release from dissolving silicate minerals. American Mineralogist, 102, 2142-2145.

Siebecker, M. G., Chaney, R. L., and Sparks, D. L. (2018) Natural speciation of nickel at the micrometer scale in serpentine (ultramafic) topsoils using microfocused X-ray fluorescence, diffraction, and absorption. Geochemical Transactions, 19, 14.

Weston, R., and Shinkle, D. A. (2013) Geology and stratigraphy of the Black Thor and Black Label chromite deposits, James Bay Lowlands, Ontario, Canada. 12th SGA Biennial Meeting Proceedings.

TABLE S2. Long-term batch experiments (6 to 9 months) between chromite nanoparticles (0.01 $molL^{-1}$) and Mn-oxide nanoparticles (Mn_3O_4, hausmannite) in the presence and absence of organic-rich soils and chamosite

500 mL Flask #	**Cr : Mn**	**$FeCr_2O_4$ [$mgkg^{-1}$]**	**Mn_3O_4 [$mgkg^{-1}$]**	**Chamosite**	**Organic-rich soil**
1	1:1	1119.2	763	0	0
2	1:5	1119.2	3814	0	0
3	1:1	1119.2	763	10g	0
4	1:5	1119.2	3814	10g	0
5	1:1	1119.2	763	0	10g
6	1:5	1119.2	3814	0	10g

Images on the characterization of the synthesized chromite nanoparticles

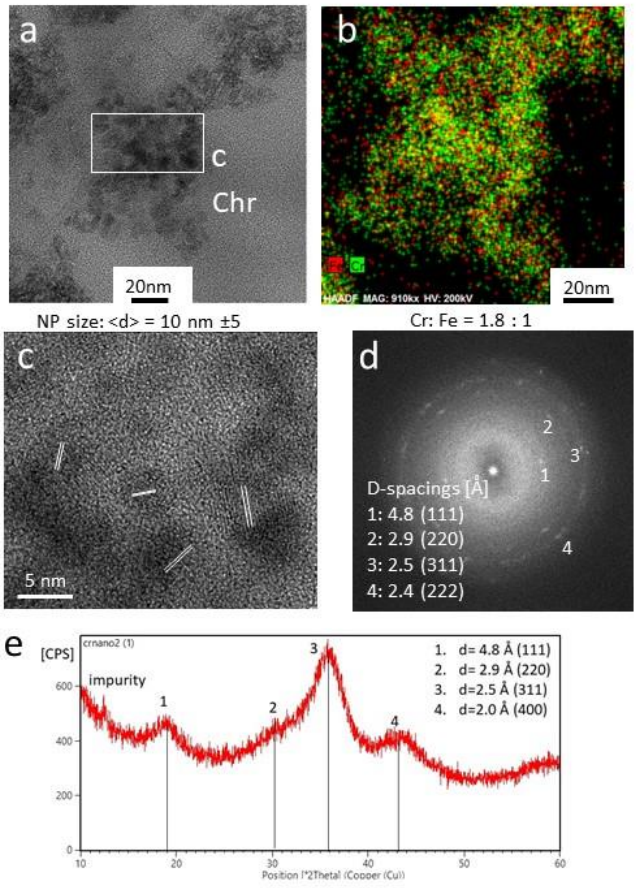

Fig, S4 **Sy**nthesized chromite (chr) nanoparticles used in the batch experiments: (a) TEM image and (b) STEM-EDS chemical distribution map for Fe (red) and Cr (green) of an aggregate of synthesized chromite nanoparticles, the area shown in (c) is indicated with a rectangle; (c) high-resolution TEM image and (d) FFT pattern of a selected area within the aggregate; the FFT pattern indicate that the lattice fringes in (c) are parallel to d=4.8 (111), d=2.9 (220), d=2.5 (311), d=2.0 (400); (e) powder diffraction pattern of the synthesized chromite nanoparticles depicting broad peaks with d-spacing similar to those observed in the FFT pattern.

STEM and TEM images of a large clinochlore colloid in the leachate of pH 5 after treatment of a silica-enriched fraction of the chromitite ore for three months

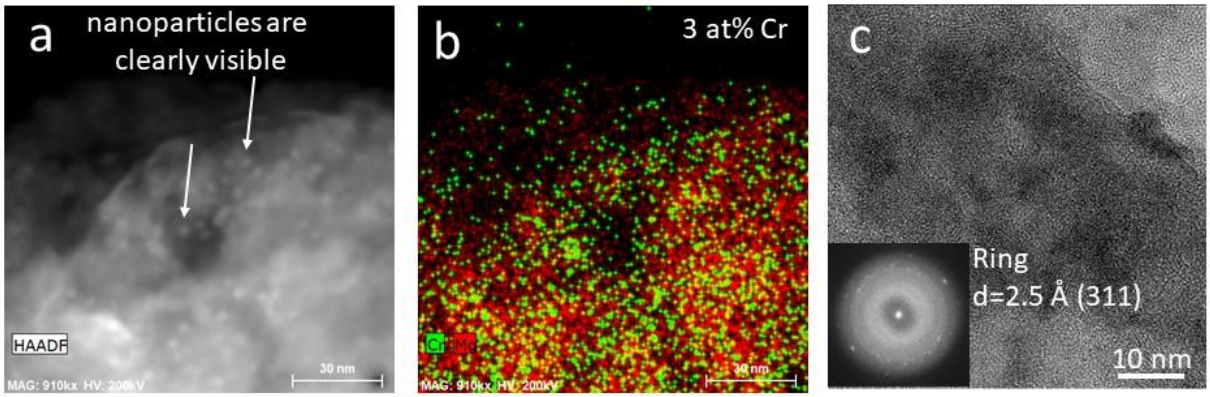

Fig S5. Large clinochlore colloid in the colloidal fraction of the leachate with pH = 5: (a) STEM image in which nanoparticles within the silicate matrix are clearly visible (bright spots); (b) EDS-STEM chemical distribution map for Cr (green) and Mg (red) and (c) high-resolution TEM image taken within the area shown in (a) and (b); the image shows the occurrence of nanoparticles (darker spots) which depict lattice fringes with characteristic d-spacings for chromite nanoparticles (d = 2.5 Å (311)

Chemical analysis of the chromite nanoparticles on the surface of an amorphous Al-rich colloid in the leachate of pH 5 after treatment of a silica-enriched fraction of the chromitite ore for three months

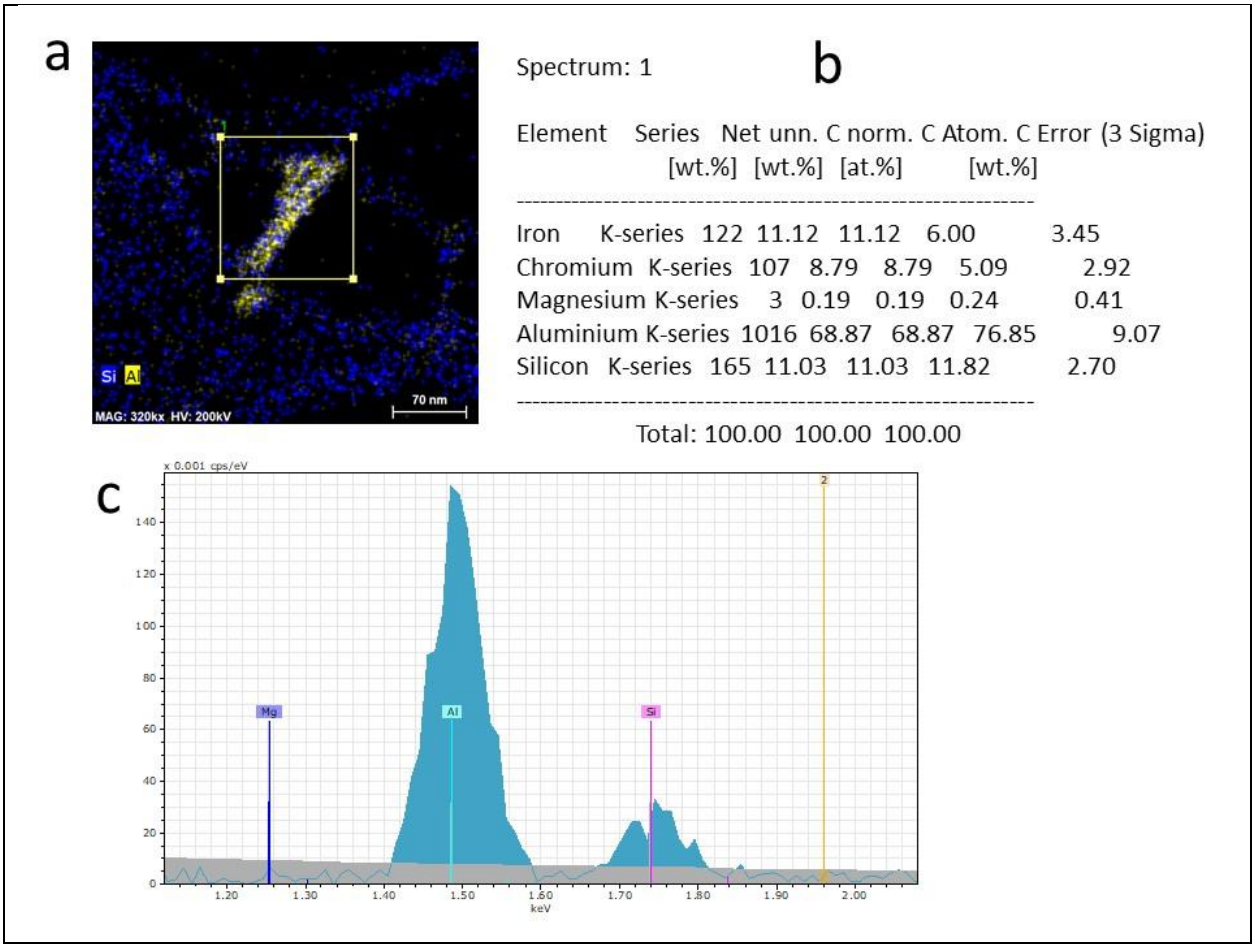

Fig. S5. (a) STEM-EDS chemical distribution map for Al (yellow) and Si (blue) of chromite nanoparticles attached to a larger Al-rich colloid; a white box indicates the area for used for the generation of an EDS spectrum; (b) corresponding semi-quantitative analyses and (2) EDS spectrum for E = 1.10 – 2.21 keV, indicating the absence of Mg in the colloid, including chromite nanoparticles.

Additional TEM data for the colloidal fraction in the suspensions after the long-term experiments

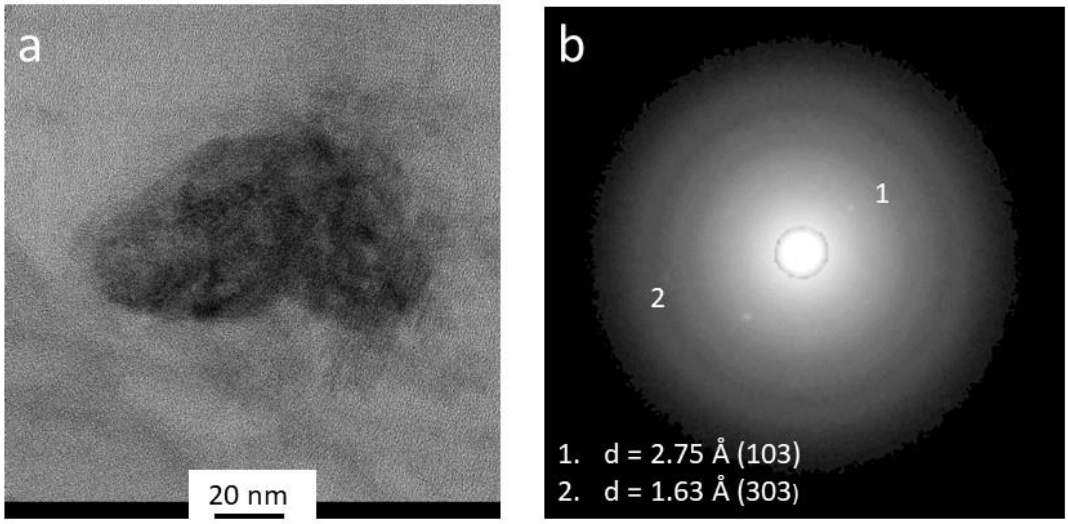

Fig. S7. (a) TEM image of two hausmannite nanoparticles
and a highly altered chromite nanoparticle; (b) SAED pattern of the aggregate depicting diffraction spots corresponding to d-spacings characteristic of hausmannite

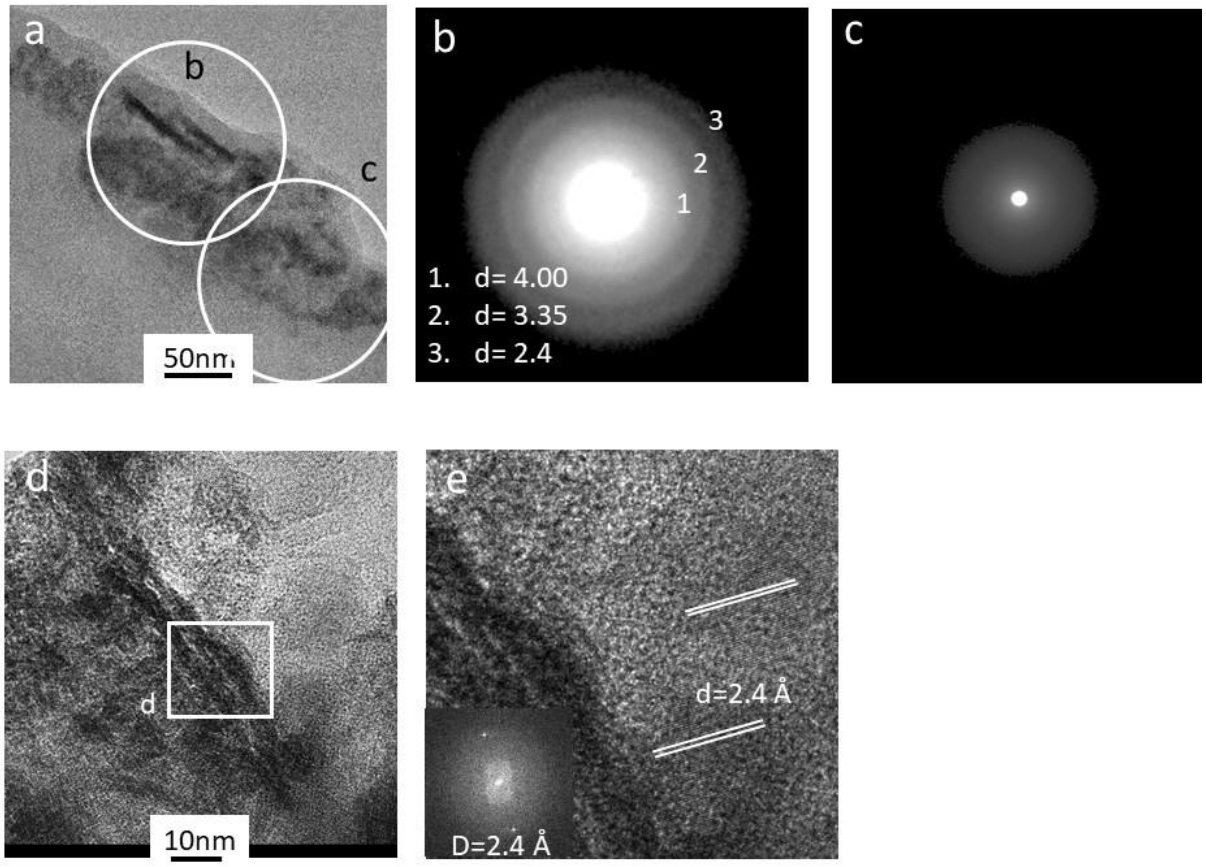

Fig. S8. (a) TEM image and (b)-(c) SAED pattern of (b) bracewellite rods (γ-CrO(OH)) and (c) surrounding matrix; circles in (a) indicate the areas from which the SAED pattern were recorded (d)-(e) TEM images of bracewellite rods and FFT pattern with characteristic d-spacings for bracewellite; a white box in (d) indicates the location of the image in (e); the FFT pattern in the lower left corner of (e) was taken from the area where the lattice fringes are highlighted with white lines.

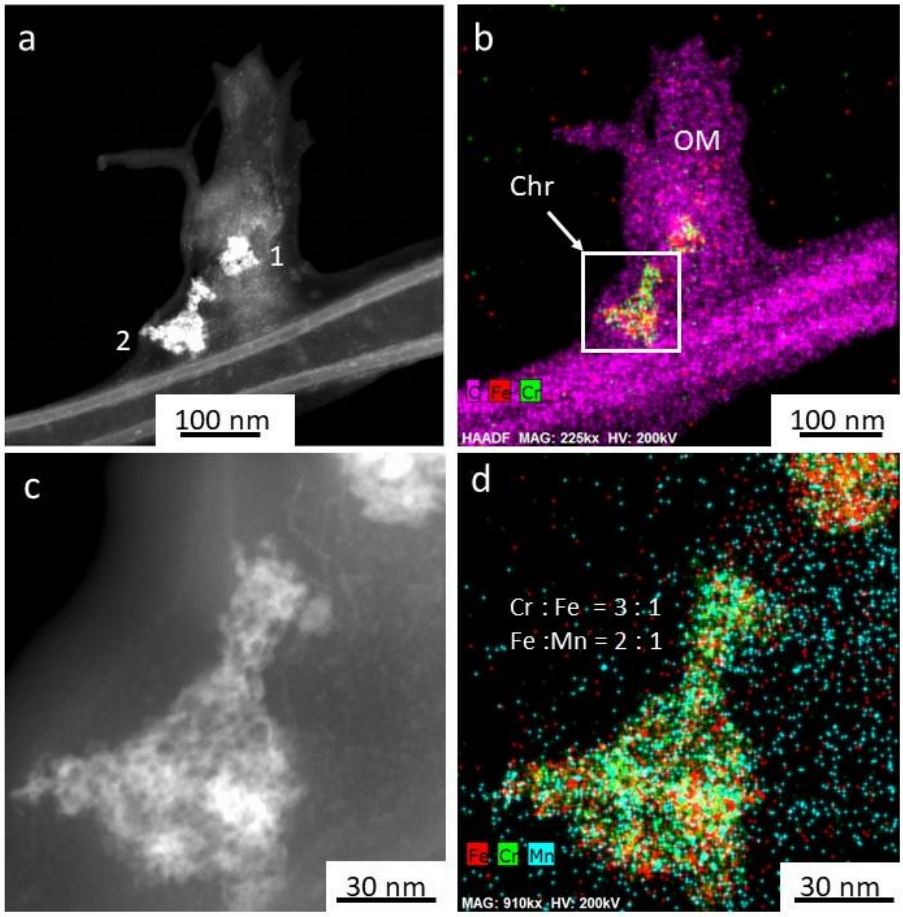

Fig. S9. (a) and (c) STEM images and (b) and (d) STEM-EDS chemical distribution maps for (b) C (purple), Fe (red) and Cr (green) and (d) Fe (red), Cr (green), Mn (blue) of aggregates of chromite nanoparticles (chr) attached to larger organic matter (OM); the area shown in (c) and (d) is depicted by a rectangle in (b); aggregate 1 is composed of weakly-altered chromite cubes whereas aggregate 2 is highly altered and is depleted in Fe and enriched in Cr and Mn relative to aggregate 1.